

Gravitationally sensitive structured x-ray optics using nuclear resonances

Shin-Yu Lee,¹ Sven Ahrens,² and Wen-Te Liao^{1,3,4,*}

¹*Department of Physics, National Central University, Taoyuan City 32001, Taiwan*

²*Shanghai Normal University, Shanghai 200234, China*

³*Physics Division, National Center for Theoretical Sciences, Taipei 10617, Taiwan*

⁴*Center for Quantum Technology, Hsinchu 30013, Taiwan*

(Dated: May 2, 2023)

Einstein's general theory of relativity not only revolutionized human understanding of the universe, but also brought many gravitational applications in large scale, such as gravitational-wave astronomy [1], gravitational lensing [2], and the operation of the global positioning system [3]. However, it still remains a challenge to implement applications for gravitational effects at small spacial extensions on Earth. Here, we investigate a structured waveguide system that allows for the control of an x-ray profile at altitude separations of millimeters and even shorter using the nuclear resonant scattering of x rays [4, 5]. Our present results suggest a potential compact scheme for turning the Earth's gravity into a practical application of x-ray optics.

The Pound–Rebka experiment [6] has demonstrated a unique system for probing the gravitational red-shift effect by exploiting an extremely narrow nuclear linewidth in combination of a high x-ray energy in the Mössbauer effect [7]. Moreover, advances in modern x-ray light sources and optics have raised the field of x-ray-nuclei interactions to a new level of accuracy where coherent quantum control comes into play [8–21]. A combination of nuclear quantum coherence and its sensitivity to gravity will potentially lead to a new type of x-ray optics whose performance depends on the gravitational red-shift in addition to the typical Zeeman shift [8, 12] and Doppler shift [14, 17–19]. In this context, we investigate a system that emulates the Schrödinger equation [22] and is sensitive to gravity. The present scheme allows for a systematic generation of structured x rays [23–26] via changing the altitude, the x-ray photon energy, or the external magnetic field of a our system for a given waveguide structure.

The system is depicted in Figure 1 with the description as follows. An x ray drives a nuclear transition from the ground state $|g\rangle$ to the excited state $|e\rangle$ with the total detuning $\Delta_t\Gamma = (\Delta_G + \Delta)\Gamma$ in Fig. 1(a). We emphasize that the gravitational red shift $\Delta_G \simeq -zE_tGM_E/(\hbar\Gamma c^2R_E^2)$ has to be taken into account when the system is located at different altitude z relative to where x rays are emitted. Here E_t is the nuclear transition energy, G is the gravitational constant, M_E is the mass of the Earth, and R_E is the average radius of the Earth. $\Delta\Gamma$ is the x-ray detuning, and Γ the spontaneous decay rate of the excited state $|e\rangle$. Our system of nuclear resonant scattering of x rays can be described by the optical-Bloch equation [9, 21]:

$$\partial_t \rho_{eg} = -\Gamma \left[\frac{1}{2} - i(\Delta + \Delta_G) \right] \rho_{eg} + \frac{i}{2} \frac{P}{\hbar} E, \quad (1)$$

$$\frac{1}{c} \partial_t E + \partial_y E = \frac{-1}{2ik} \nabla_{\perp}^2 E - \frac{k}{2i} (n_e^2 - 1) E + i\eta \rho_{eg}, \quad (2)$$

where ρ_{eg} is the coherence of a nuclear two-level system, E is the x-ray electric field strength, \hbar is the reduced Planck constant, k is the x-ray wavenumber, and n_e is the index

of refraction from electrons. Further, we denote the transverse Laplacian $\nabla_{\perp}^2 = \partial_x^2 + \partial_z^2$, and the coupling constant $\eta = 2\hbar\Gamma\xi/(PL)$, where L the length of the waveguide, P is the nuclear transition dipole moment, and ξ is the nuclear resonant thickness. The steady state of Eqs. (1-2) leads to the analytic solution $\rho_{eg} = PE(i - 2\Delta_t)/[\hbar\Gamma(1 + 4\Delta_t^2)]$ and the optical Schrödinger equation [22] (see supplemental information)

$$i\hbar c \partial_y E = -\frac{\hbar^2}{2m_e} \nabla_{\perp}^2 E + \hbar c \left[\frac{k(1 - n_e^2)}{2} + \frac{4\xi\Delta_t}{L(1 + 4\Delta_t^2)} \right] E, \quad (3)$$

with the effective mass $m_e = \hbar k/c$. Equation (3) suggests a structured x-ray waveguide (SXWG) system composed of resonant nuclei, as depicted in Fig. 1(b), with a high degree of freedom for simulating different quantum systems via spatial engineering of n_e and ξ . Fig. 1(c) displays the altitude dependent real part $Re[\rho_{eg}]$ (blue-solid) and imaginary part $Im[\rho_{eg}]$ (red-dashed line) of ρ_{eg} with $\Delta = 0$ for the isotope ^{45}Sc . $Re[\rho_{eg}]$ describes the refractive index from nuclei and results in the gravitational effects in our system as revealed by the last term of Eq. (3). In contrast, $Im[\rho_{eg}]$ of Lorentzian line shape represents the nuclear absorption of x rays and leads to the Pound–Rebka experiment [6].

In the following, we use the SXWG to simulate Rabi oscillations of x ray in a finite square well of width L_x . As illustrated in Fig. 1(d), we introduce a platinum cladding $n_e = 1 - \delta_{\text{Pt}} + i\beta_{\text{Pt}}$ for $|x| > L_x/2$ to constitute a finite square well potential, which provides with a transverse confinement to the x ray propagation direction [21]. The cladding material leads to the energy eigenfunctions of the E field in Eq. (3) which read as (see supplemental information)

$$\psi_n(x) = \sqrt{\frac{2}{L_x}} \sin \left[\frac{n\pi}{L_x} \left(x + \frac{L_x}{2} \right) \right], \quad (4)$$

with the eigen angular frequencies $\omega_n = n^2\pi^2c/(2kL_x^2)$. Inside the square well $|x| \leq L_x/2$, we perturb the system by a periodic (gradient) particle distribution of isotope X and carbon along the y direction (x direction), where $\xi(x, y) = (\varrho/2)[1 + (2x/L_x)\sin(k_d y)]$ and $n_e(x, y) = 1 - \delta_C(x, y) + i\beta_C(x, y) - \delta_X(x, y) + i\beta_X(x, y)$ (see supplemental information for the form of n_e). In Fig. 1(d) subscripts Pt, C, and X

TABLE I. **Nuclear and waveguide material parameters.** For each isotope X we present the nuclear transition energy E_t and the radiative decay rate Γ . The last six columns list the x-ray index of refraction $n_e = 1 - \delta + i\beta$ for SXWG materials [5, 27, 28].

X	E_t (keV)	Γ (MHz)	$\delta_X(10^{-6})$	$\delta_C(10^{-6})$	$\delta_{Pt}(10^{-5})$	$\beta_X(10^{-9})$	$\beta_C(10^{-9})$	$\beta_{Pt}(10^{-6})$
^{45}Sc	12.4	2.18×10^{-6}	3.84	2.97	2.091	131.9	1.78	2.737
^{57}Fe	14.413	7.05	7.43	2.20	1.607	338.9	0.93	2.49
^{73}Ge	13.275	0.24	5.41	2.59	1.622	508.9	1.32	2.947
^{181}Ta	6.238	0.11	67.74	11.77	8.731	7987.3	32.76	12.616
^{182}Ta	16.273	2.45×10^{-6}	10.41	1.72	1.304	1062.2	0.55	1.642

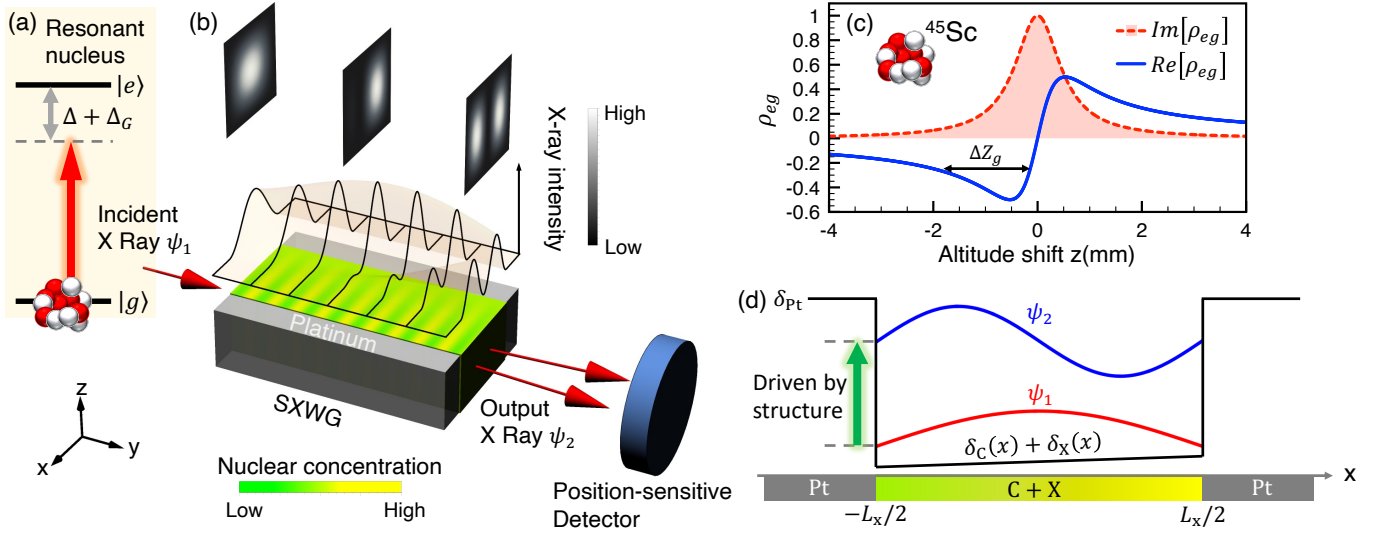


FIG. 1. (a) the incident x ray (red upward arrow) drives a nuclear transition $|g\rangle \rightarrow |e\rangle$ with detuning $\Delta + \Delta_G$ (gray vertical double arrows). Δ is the x-ray detuning, and Δ_G is the x-ray gravitational red shift. (b) a hard x ray of transverse mode ψ_1 (red arrow) propagates through a structured platinum cladding waveguide with a periodic nuclear distribution whose spatial concentration is indicated by the horizontal green-yellow legend. An output x ray of mode ψ_2 is measured by a downstream position-sensitive detector (blue thick disc). The top black curves and pictures in gray level represent the intra-waveguide x-ray intensity. (c) the SXWG altitude-dependent nuclear coherence ρ_{eg} between the nuclear ground state $|g\rangle$ and the excited state $|e\rangle$ of the isotope ^{45}Sc . Red-dashed (blue-solid) line depicts the imaginary (real) part of the nuclear ρ_{eg} . Black horizontal double arrow indicates the full altitude width ΔZ_G at the half maximum $|Re[\rho_{eg}]|$. (d) the transversely gradient (along x) and the longitudinally periodic (along y) electronic refractive index of an SXWG. Between the platinum claddings the intra-waveguide structure, made of carbon and an isotope X , drives the transition from the x-ray ground state ψ_1 (red-solid line) to the first excited state ψ_2 (blue-solid line).

represent platinum, carbon and resonant nucleus, respectively. We list other relevant material parameters in Table I. With the above density modulation, the last term in Eq. (3) effectively becomes the electric dipole Hamiltonian in an oscillating field which perturbs the square well potential. This plays the key role to drive the x-ray Rabi oscillation with gravitational sensitivity. When the resonant condition $ck_d = \omega_{n+1} - \omega_n$ is fulfilled, the periodic structure of the refractive index drives the dipole transition $\psi_n \rightarrow \psi_{n+1}$ with the effective Rabi frequency (see supplemental information)

$$\Omega_n = \frac{16gn(n+1)c}{\pi^2(2n+1)^2L} \left[\frac{k(\delta_C - \delta_{Sc})}{2N\sigma_0} + \frac{2\Delta_t}{1+4\Delta_t^2} \right]. \quad (5)$$

A propagating x ray experiences a constant SXWG-induced Rabi frequency, and the condition for having a $m\pi$ pulse is $|\Omega_n|L/c = m\pi$. We use $m = 2$ to demonstrate the Rabi oscillation between the x-ray ground state ψ_1 and the first excited state ψ_2 by numerically solving Eq. (3).

The solution of Eq. (3) in Fig. 2 represents an x ray which propagates through an SXWG with $X = {}^{45}\text{Sc}$, $\rho = 26.25$, natural scandium particle density $N = 3.99 \times 10^{28} \text{m}^{-3}$, nuclear resonance absorption cross section $\sigma_0 = 12.6(\text{kbarn})$, $L_x = 100 \text{nm}$, $L = 4 \text{mm}$, $k_d = 22.778 \times 10^3 \text{rad/m}$, $\Delta = 4\Gamma$, and $\Delta_G = 0$. The process is visualized in terms of the fidelity $F_n(y) = |\int_{-\infty}^{\infty} \psi_n^*(x) E(x, y) dx|^2 / \int_{-\infty}^{\infty} |E(x, y)|^2 dx$ in Fig. 2(a), and the normalized intra-waveguide x-ray intensity distribution $|E(x, y)|^2 / \int_{-\infty}^{\infty} |E(x, y)|^2 dx$ in Fig. 2(b). The alternation of F_1 and F_2 in Fig. 2(a) clearly demonstrates that the ground-state x ray enters the SXWG at $y = 0$, and is then coherently promoted to the first excited state when approaching $y = 2 \text{mm}$. After that, the x ray returns to the ground state and

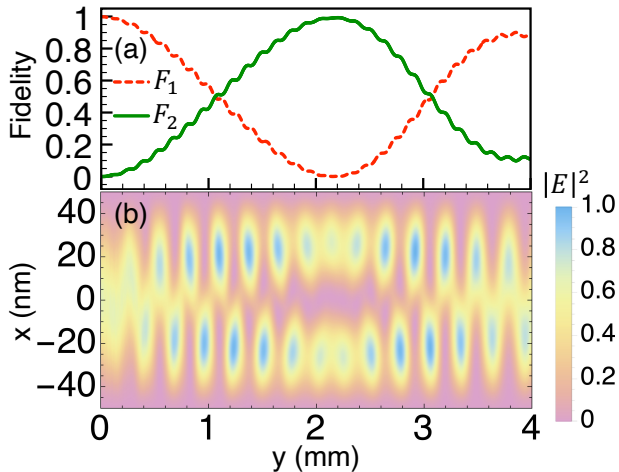


FIG. 2. A full cycle of the x-ray Rabi oscillation between ψ_1 and ψ_2 is illustrated by (a) the fidelity F_1 (red-dashed line) and F_2 (green-solid line) and (b) the normalized intra-waveguide x-ray intensity distribution. The input x-ray in the state ψ_1 splits and reaches the maximum transverse double-hump separation of the state ψ_2 at $y = 2 \text{mm}$ where the maximum F_2 also occurs. For $y > 2 \text{mm}$ the x-ray confluence reflects the second half Rabi cycle, and the transverse x-ray pattern returns toward the state ψ_1 .

finishes a full Rabi cycle at $y = 4 \text{mm}$. One can also observe the same phenomenon at the intra-waveguide x-ray intensity which evolves back and forth between states ψ_1 and ψ_2 in Fig. 2(b).

The above x-ray Rabi oscillation suggests a systematic way to generate the ψ_n mode with a sequence of SXWGs driving $\Delta n = 1$ transitions, where one can raise the quantum number one by one. Specifically, one can connect two different SXWGs to accomplish a $\psi_1 \rightarrow \psi_3$ transition, where the upstream SXWG drives a $\psi_1 \rightarrow \psi_2$ transition, and the downstream SXWG achieves a $\psi_2 \rightarrow \psi_3$ promotion. Moreover, one can even design multiple SXWG modules for $\Delta n = 2$ or any dipole forbidden transitions. Thus, all combinations of SXWG modules open the capability to generate high order x-ray modes starting from the ground state ψ_1 . It is worth mentioning another possible application using dual SXWGs with a gap in between as an x-ray interferometer. While the upstream SXWG causes the $\psi_1 \rightarrow \psi_2$ transition as a beam splitter, the downstream SXWG leads to the return of $\psi_2 \rightarrow \psi_1$ as a beam combiner. Furthermore, in the gap between two SXWGs one can introduce a phase modulator to impose a phase shift at one branch of the split state ψ_2 , e.g., $x > 0$ at $y = 2 \text{mm}$ in Fig. 2. A controllable interference due to the phase modulation is expected to happen at the end of the downstream SXWG.

We are ready to demonstrate the Earth's gravitational effect on our SXWG system. Given that the gravitational redshift Δ_G significantly changes the nuclear coherence ρ_{eg} and Rabi frequency Ω_n in Eq. (5) in two millimeter on Earth as demonstrated in Fig. 1(c), this sensitivity potentially allows for turning gravity into a practical use, e.g., gravitationally sensitive x-ray optics. For illustrating the effect, we numerically solve Eq. (3) and use the isotope ${}^{45}\text{Sc}$ in an SXWG with parameters $\rho = 8.38$, $L_x = 100 \text{nm}$, $L = 2 \text{mm}$, $k_d = 23.778 \times 10^3 \text{rad/m}$, and $\Delta = 19.36$ to show the gravitational effect. Fig. 3(a) illustrates three cases where the above discussed SXWG is located at $z = 2.32 \text{cm}$, $z = 2 \text{cm}$, and $z = 1.72 \text{cm}$ from the top down. An incident x ray with the transverse mode ψ_1 is deflected upward and experiences a gravitational redshift (vertical upward arrow with color gradient). The Δ_G will change when the x ray illuminates the SXWG at different altitudes. The total detuning for each case is specified at the level-scheme plot, namely, $\Delta + \Delta_G = -2.52$, $\Delta + \Delta_G = 0.5$, and $\Delta + \Delta_G = 3.14$ from the top down. We emphasize that the periodic particle density modulation effectively plays the role of a resonant field, and it always resonantly drives a transition between the x-ray modes in a cladding waveguide for three cases. However, various Δ_G change the effective coupling strength Ω_n and result in different outputs. The scattered/split x rays reflect the output mode and can be measured by a downstream position-sensitive detector. The x -dependent photon number counts show the output $|E(x, L)|^2$ and reveal the Earth's gravitational effect. We depict the normalized $|E(x, y)|^2$ for $z = 2.32 \text{cm}$, $z = 2 \text{cm}$, and $z = 1.72 \text{cm}$ in Fig. 3(c, e, and g), respectively. The intra-waveguide intensity shows that the x ray significantly gets split in Fig. 3(e) under a half Rabi cycle $\psi_1 \rightarrow \psi_2$ in the SXWG at $z = 2 \text{cm}$. In contrast, Fig. 3(c and g) depicts only a transverse broad-

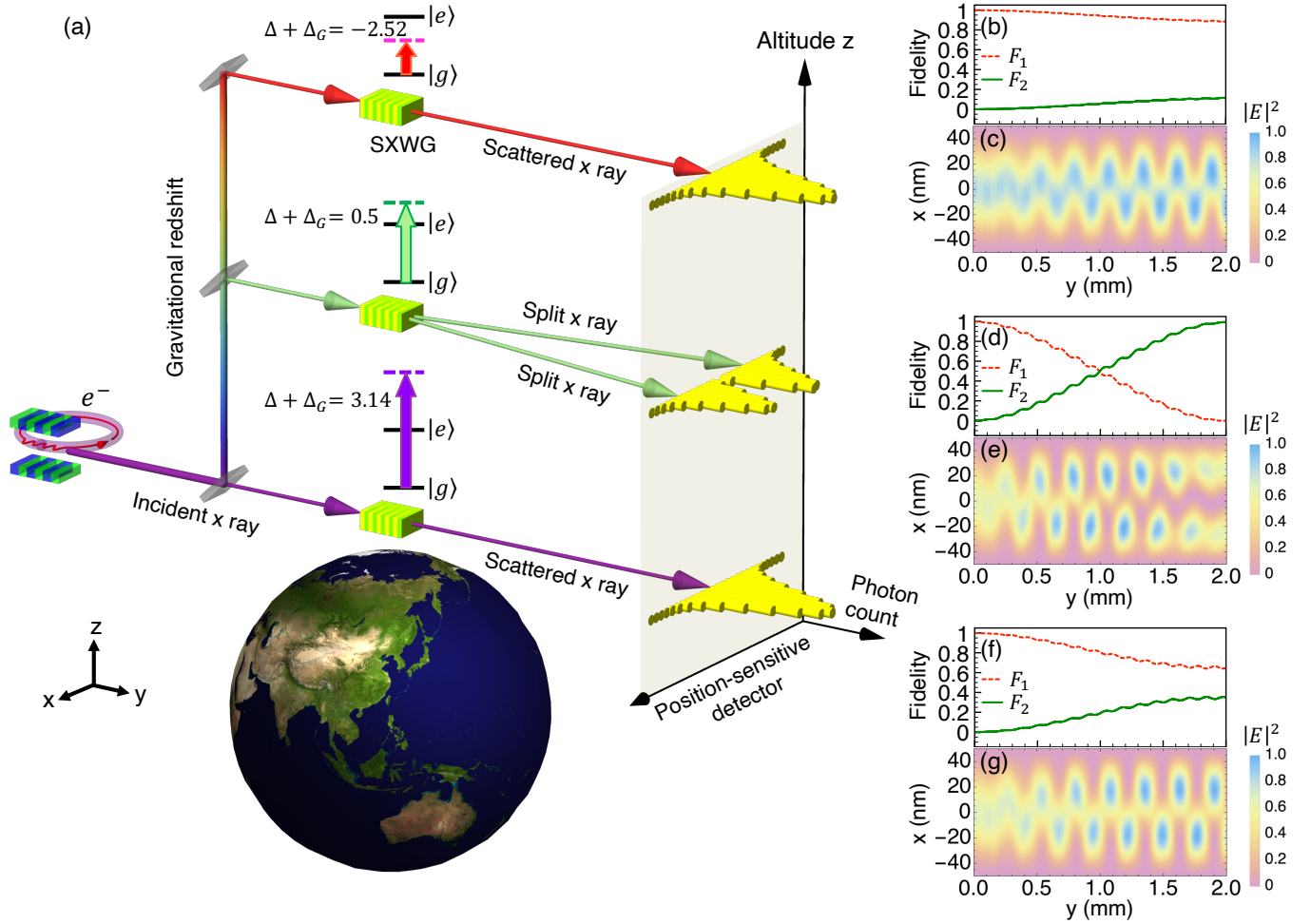


FIG. 3. (a) Earth's gravity changes the x-ray propagation in the waveguide composed of ^{45}Sc nuclei. Three cases at different altitudes $z = 2.32\text{cm}$, $z = 2\text{cm}$, and $z = 1.72\text{cm}$ where x rays propagate with a detuning $\Delta = 19.36$ and gravitational red shifts $\Delta_G = -21.88$, $\Delta_G = -18.86$, and $\Delta_G = -16.22$, respectively. (b, d, and f) the fidelity F_1 (red-dashed line) and F_2 (green-solid line) for $z = 2.32\text{cm}$, $z = 2\text{cm}$, and $z = 1.72\text{cm}$, respectively. (c, e, and g) the normalized intra-waveguide x-ray intensity distribution $|E(x, y)|^2$ at altitude $z = 2.32\text{cm}$, $z = 2\text{cm}$, and $z = 1.72\text{cm}$ from the top to the bottom.

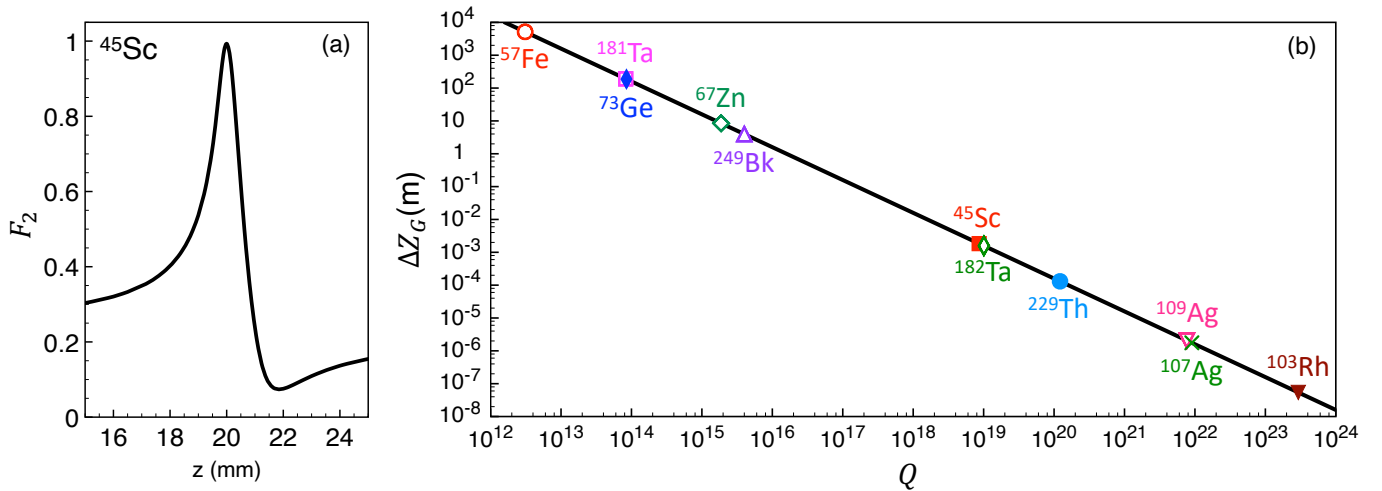


FIG. 4. (a) altitude-dependent x-ray fidelity F_2 through an SXWG composed of ^{45}Sc nuclei. (b) the FWHM ΔZ_G on Earth is dependent on the quality factor Q of nuclear resonances for different nuclear species.

ening of the x ray due to a small $|\Omega_1|$. Fig. 3(b,d, and f) illustrate $F_1(y)$ (red-dashed line) and $F_2(y)$ (green-solid line) for $z = 2.32\text{cm}$, $z = 2\text{cm}$, and $z = 1.72\text{cm}$, respectively. One can clearly see that the x ray experiences Rabi flopping and becomes ψ_2 at the resonant altitude $z = 2\text{cm}$ as also pointed out by Fig. 3(d and e). Given that $|\Omega_1|$ decreases when the SXWG leaves the resonant altitude, the x ray mostly remains in the initial mode ψ_1 , namely, $F_1(y) > F_2(y)$ at $z = 2.32\text{cm}$ and $z = 1.72\text{cm}$. We depict the output altitude-dependent F_2 at $y = 2\text{mm}$ in Fig. 4(a). As a result, different x-ray splitting is expected to occur when lifting an SXWG composed of ^{45}Sc at only a millimeter altitude change.

We quantify the gravitational sensitivity of the SXWG by the full altitude width ΔZ_G at the half maximum $Re[\rho_{eg}]$

$$\Delta Z_G = \sqrt{3} \left(\frac{\hbar\Gamma}{E_t} \right) \frac{c^2 R_E^2}{GM_E}, \quad (6)$$

as indicated by the black-horizontal double arrow in Fig. 1(c). The introduced ΔZ_G is a measure for the sensitivity of the x-ray-nucleus coupling to the change of the SXWG vertical location. With the definition of the quality factor of a nuclear resonance $Q = E_t/(\hbar\Gamma)$, we can see that ΔZ_G is proportional to $1/Q$. Fig. 4(b) exemplifies the implication of Eq. (6) for our system on Earth in a double-logarithmic plot, where we mark the isotopes ^{45}Sc , ^{57}Fe , ^{67}Zn , ^{73}Ge , ^{103}Rh , ^{107}Ag , ^{109}Ag , ^{181}Ta , ^{182}Ta , ^{229}Th , and ^{249}Bk , according their Q factor. Some of the nuclear parameters are listed in Table I. Remarkably, the advantage of a very high $Q \sim 10^{19}$ of ^{45}Sc or ^{182}Ta nuclear resonance endues an SXWG with a gravitational sensitivity to only millimeter altitude change. Notably, it is also possible to get sub-millimeter ΔZ_G using ^{229}Th whose $Q \sim 10^{20}$ [29], and micron ΔZ_G with ^{107}Ag and ^{109}Ag whose $Q \sim 10^{22}$. It deserves to mention that ^{103}Rh whose $Q > 10^{23}$ [27] even results in a nanometer ΔZ_G , and it may lead to gravitational application in mesoscopic scale.

In conclusion we have put forward a controllable SXWG system that potentially turns gravity into an application of x-ray optics. A periodic intra-waveguide structure, e.g., nuclear optical lattice $^{57}\text{Fe}/^{56}\text{Fe}$ bilayers in Ref.[30], can drive a transition between x-ray modes. The x-ray transverse mode experiences Rabi oscillation when propagating in an SXWG. Our scheme allows for applications like a systematic production of structured x rays and an x-ray interferometer without any beam splitter. Remarkably, a significant change of a gravitationally induced splitting of x rays could happen by lifting our SXWG made of, e.g., ^{45}Sc or ^{182}Ta , at only a millimeter scale.

S.-Y. L. and W.-T. L. are supported by the National Science and Technology Council of Taiwan (Grant No. 110-2112-M-008-027-MY3, 110-2639-M-007 -001-ASP, 111-2923-M-008-004-MY3 & 111-2639-M-007-001-ASP). S. A. is supported by National Science Foundation of China (Grant No. 11975155).

- [1] B. P. Abbott and et al. (LIGO Scientific Collaboration and Virgo Collaboration), Observation of gravitational waves from a binary black hole merger, *Phys. Rev. Lett.* **116**, 061102 (2016).
- [2] M. Bartelmann and P. Schneider, Weak gravitational lensing, *Physics Reports* **340**, 291 (2001).
- [3] N. Ashby, Relativity and the global positioning system, *Physics Today* **55**, 41 (2002).
- [4] J. B. Hastings, D. P. Siddons, U. van Bürck, R. Hollatz, and U. Bergmann, Mössbauer spectroscopy using synchrotron radiation, *Phys. Rev. Lett.* **66**, 770 (1991).
- [5] R. Röhlsberger, *Nuclear Condensed Matter Physics With Synchrotron Radiation: Basic Principles, Methodology and Applications* (Springer-Verlag, 2004).
- [6] R. V. Pound and G. A. Rebka, Apparent weight of photons, *Phys. Rev. Lett.* **4**, 337 (1960).
- [7] M. Kalvius and P. Kienle, *The Rudolf Mössbauer Story: His Scientific Work and Its Impact on Science and History* (Springer Science & Business Media, 2012).
- [8] Y. V. Shvyd'ko, T. Hertrich, U. van Bürck, E. Gerdau, O. Leupold, J. Metge, H. D. Rüter, S. Schwendy, G. V. Smirnov, W. Potzel, and P. Schindelmann, Storage of nuclear excitation energy through magnetic switching, *Phys. Rev. Lett.* **77**, 3232 (1996).
- [9] Y. V. Shvyd'ko, Nuclear resonant forward scattering of x rays: Time and space picture, *Phys. Rev. B* **59**, 9132 (1999).
- [10] A. Pálffy, C. H. Keitel, and J. Evers, Single-photon entanglement in the kev regime via coherent control of nuclear forward scattering, *Phys. Rev. Lett.* **103**, 017401 (2009).
- [11] R. Röhlsberger, H. C. Wille, K. Schlage, and B. Sahoo, Electromagnetically induced transparency with resonant nuclei in a cavity, *Nature* **482**, 199 (2012).
- [12] W.-T. Liao, A. Pálffy, and C. H. Keitel, Coherent storage and phase modulation of single hard-x-ray photons using nuclear excitons, *Phys. Rev. Lett.* **109**, 197403 (2012).
- [13] B. W. Adams, C. Buth, S. M. Cavaletto, J. Evers, Z. Harman, C. H. Keitel, A. Pálffy, A. Picón, R. Röhlsberger, Y. Rostovtsev, and K. Tamasaku, X-ray quantum optics, *Journal of modern optics* **60**, 2 (2013).
- [14] F. Vagizov, V. Antonov, Y. Radeonychev, R. N. Shakhmuratov, and O. Kocharovskaya, Coherent control of the waveforms of recoilless γ -ray photons, *Nature* **508**, 80 (2014).
- [15] W.-T. Liao and S. Ahrens, Gravitational and relativistic deflection of x-ray superradiance, *Nature Photonics* **9**, 169 (2015).
- [16] K. P. Heeg, J. Haber, D. Schumacher, L. Bocklage, H.-C. Wille, K. S. Schulze, R. Loetzsch, I. Uschmann, G. G. Paulus, R. Ruffer, R. Röhlsberger, and J. Evers, Tunable subluminal propagation of narrow-band x-ray pulses, *Phys. Rev. Lett.* **114**, 203601 (2015).
- [17] K. P. Heeg, A. Kaldun, C. Strohm, P. Reiser, C. Ott, R. Subramanian, D. Lentrodt, J. Haber, H.-C. Wille, S. Goerttler, R. Ruffer, C. H. Keitel, R. Röhlsberger, T. Pfeifer, and J. Evers, Spectral narrowing of x-ray pulses for precision spectroscopy with nuclear resonances, *Science* **357**, 375 (2017).
- [18] X. Zhang, W.-T. Liao, A. Kalachev, R. Shakhmuratov, M. Scully, and O. Kocharovskaya, Nuclear quantum memory and time sequencing of a single γ photon, *Phys. Rev. Lett.* **123**, 250504 (2019).
- [19] Y. V. Radeonychev, I. R. Khairulin, F. G. Vagizov, M. Scully, and O. Kocharovskaya, Observation of acoustically induced transparency for γ -ray photons, *Phys. Rev. Lett.* **124**, 163602 (2020).
- [20] K. P. Heeg, A. Kaldun, C. Strohm, C. Ott, R. Subramanian, D. Lentrodt, J. Haber, H.-C. Wille, S. Goerttler, R. Ruffer, et al., Coherent x-ray-optical control of nuclear excitons, *Nature* **590**, 401 (2021).

* wente.liao@g.ncu.edu.tw

- [21] Y.-H. Chen, P.-H. Lin, G.-Y. Wang, A. Pálffy, and W.-T. Liao, Transient nuclear inversion by x-ray free electron laser in a tapered x-ray waveguide, *Phys. Rev. Research* **4**, L032007 (2022).
- [22] M. A. M. Marte and S. Stenholm, Paraxial light and atom optics: The optical schrödinger equation and beyond, *Phys. Rev. A* **56**, 2940 (1997).
- [23] D. Seipt, A. Surzhykov, and S. Fritzsche, Structured x-ray beams from twisted electrons by inverse compton scattering of laser light, *Phys. Rev. A* **90**, 012118 (2014).
- [24] H. Rubinsztein-Dunlop, A. Forbes, M. V. Berry, M. R. Dennis, D. L. Andrews, M. Mansuripur, C. Denz, C. Alpmann, P. Banzer, T. Bauer, *et al.*, Roadmap on structured light, *Journal of Optics* **19**, 013001 (2016).
- [25] C. A. MacDonald, Structured x-ray optics for laboratory-based materials analysis, *Annual Review of Materials Research* **47**, 115 (2017).
- [26] A. Forbes, M. de Oliveira, and M. R. Dennis, Structured light, *Nature Photonics* **15**, 253 (2021).
- [27] *National Nuclear Data Center*, <https://www.nndc.bnl.gov/ensdf/>.
- [28] *The Center for X-Ray Optics*, <https://www.cxro.lbl.gov/>.
- [29] B. Seiferle, L. von der Wense, P. V. Bilous, I. Amersdorffer, C. Lemell, F. Libisch, S. Stellmer, T. Schumm, C. E. Düllmann, A. Pálffy, *et al.*, Energy of the 229th nuclear clock transition, *Nature* **573**, 243 (2019).
- [30] J. Haber, K. S. Schulze, K. Schlage, R. Loetzsch, L. Bocklage, T. Gurieva, H. Bernhardt, H.-C. Wille, R. Rüffer, I. Uschmann, *et al.*, Collective strong coupling of x-rays and nuclei in a nuclear optical lattice, *Nature Photonics* **10**, 445 (2016).